XXI IMEKO World Congress "Measurement in Research and Industry"
August 30 – September 4, 2015, Prague, Czech Republic

EXPERIMENTAL INVESTIGATION OF COMPUTED TOMOGRAPHY DIMENSIONAL CAPABILITY USING MODULAR TEST ARTEFACTS

Crhistian Raffaelo Baldo [1], *Thiago Linhares Fernandes* [1], *Gustavo Daniel Donatelli* [1]

[1] Reference Centers in Innovative Technologies (CERTI Foundation), Center for Metrology and Instrumentation, Florianópolis, Santa Catarina, Brazil, cb@certi.org.br

Abstract – Computed tomography for dimensional metrology has been introduced in quality control loop for about a decade. Due to the complex measurement-error cause system, usually no consistent uncertainty reporting has been made. Modular test parts have been developed and used to investigate some influence factors intrinsic to CT-based data and their effects on checking features of size. The experimental planning and the most significant findings are outlined and discussed in this paper.

Keywords: computed tomography, measurement uncertainty, features of size, modular test artefacts

1. INTRODUCTION

Computed tomography (CT) for coordinate metrology has been part of dimensional quality control for about a decade. In general, complex-shaped parts with hundreds (or even thousands) of features can be holistically inspected with great operational advantages over other existing technologies. CT measurement principle relies on the attenuation of X-rays when propagating through the part, which depends on the part material and radiographic length. For a large number of beam directions, the intensity distribution of the remaining radiation is determined and digitally stored as a grey-value image. The resulting projections of full part rotation are mathematically processed to form the 3D voxel data. Further processing steps over the voxel data allow performing dimensional checks.

Typical design of metrological CT scanners comprises the X-ray source at one end and the flat panel detector at the other. Between them, a turntable for stepwise rotation of the part is placed, which can be linearly moved along the magnification axis. Many factors may influence the quality of dimensional measurements, related to the source (e.g. photon energy, focal spot size), detector (e.g. sensitivity, pixel size, exposure time, averaging), part (e.g. material, geometry), CT kinematics (e.g. magnification axis and turntable accuracy and repeatability), and mathematical data processing (e.g. surface determination, measuring strategy) [1].

Due to the intricate measurement-error cause system and absence of a convenient method to evaluate the uncertainty of CT-based measurements, no consistent uncertainty reporting has been made thus far. To handle this matter, particularly for features of size and distances, massively presented in plastic parts received for dimensional analysis, modular test artefacts have been developed and measured in order to investigate the error behaviour of CT-based measurement data. This paper presents and discusses the experimental design and the most significant findings of this exploratory study.

2. EXPERIMENT PLANNING

Despite the large amount of factors that may contribute to data inaccuracy, from the dimensional metrology perspective, somehow they interact with each other to produce edge offset errors, magnification errors, localized structures, and random errors [2]. Fig. 1 illustrates the modular test artefacts designed for studying those effects [3]. Each artefact consists of two cylindrical surfaces (internal and external) for quantifying random errors and edge offset errors; one pattern of four holes for separating edge offset errors from the magnification errors; and threaded pins with different diameters to allow varying the penetration length without changing the intrinsic characteristics under analysis (subsection 2.1).

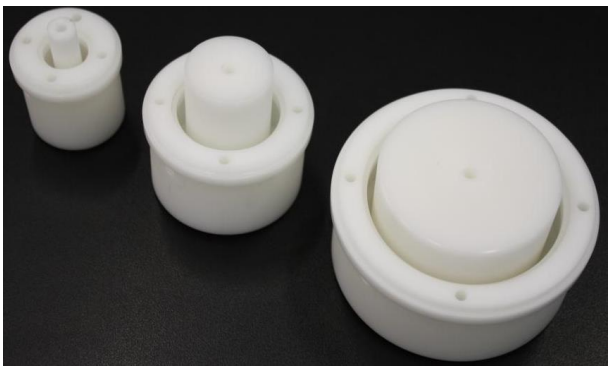

Fig. 1. Set of three modular test artefacts made of POM used to investigate the error behaviour of CT-based data.

2.1. Intrinsic characteristics under analysis

Considering the artefact design and study particularities, the following intrinsic characteristics were specified:

a) Diameter of the external circumferential line at surface mid-height, D_1;
b) Diameter of the internal circumferential line at surface mid-height, D_2;
c) Diameter of the circle associated to centres of the hole pattern, D_3;
d) Form of the external circumferential line at surface mid-height, R_1;
e) Form of the internal circumferential line at surface mid-height, R_2.

2.2. Reference measurements

The intrinsic characteristics of each modular test artefact were calibrated on a Carl Zeiss PRISMO ultra coordinate measuring machine housed in a temperature-controlled room maintained at (20.0 ± 0.3) °C. All diameters were realized by associating ideal features of type circle to the scanned points using the least-squares association method. The root-mean-square roundness error was used to estimate the form errors listed in 2.1 (filtering not applied). Measurement uncertainties were estimated using the Virtual CMM software output and expert judgment. Table 1 summarizes the calibration results.

Table 1. Calibration results for the intrinsic characteristics of each artefact (best estimates and expanded uncertainties in millimeters).

Intrinsic Characteristic	POM40	POM60	POM90
D_1	39.9236 ± 0.0015	60.0145 ± 0.0015	90.1972 ± 0.0015
D_2	16.2692 ± 0.0015	36.4101 ± 0.0015	65.9199 ± 0.0015
D_3	28.0062 ± 0.0025	47.9945 ± 0.0025	77.8573 ± 0.0025
R_1	0.0012 ± 0.0010	0.0016 ± 0.0010	0.0028 ± 0.0010
R_2	0.0011 ± 0.0010	0.0026 ± 0.0010	0.0031 ± 0.0010

2.3. Study setup

The metrological CT system investigated was a Carl Zeiss METROTOM 1500, which is equipped with a 225 kV micro-focus tube and a 2048^2 pixels flat panel detector. Due to the dimensional metrology application, the CT system is housed in a temperature-controlled laboratory kept at (20 ± 1) °C. The CT system manufacturer states a maximum permissible error for length measurements of (9 + L/50) µm, using a test piece consisting of 27 ruby spheres mounted on carbon fibre shafts, and then determining the sphere-centre to sphere-centre distances of several pairs of spheres [4]; which on the other hand disregards the material influence [5].

The study setup consisted of measuring the artefacts many times, varying some of the CT control settings or influencing factors that could be chosen or influenced by the CT operator, and then evaluating their effects on the measured features' dimensional content. Table 2 lists the CT control parameters and values used for each artefact. Setups labelled as .01 carry the base parametrization, from which conditions that change the focal spot size and the voxel size were modified, such as: source current; detector integration time, gain, and resolution; magnification factor and number of projections. Acquisition time and dataset size may also be affected by varying them, which may be a factor in some applications.

For the base parameterization, the magnification axis was positioned to project the artefact using the maximum possible area of the detector (thus reducing the voxel size). The source voltage was set high enough to avoid beam extinction, and detector integration time and gain set to convenient values. The source current was then tuned to enhance image contrast and brightness. The number of angular poses was selected as approximately the number of pixel covered by the shadow of the artefact in the projection. When adding pins to modify the penetration length, adjustments in source voltage and current were made to properly redefine the grey value distribution.

Regarding the surface definition from the voxel dataset, the standard 'iso-50%' threshold value was applied globally. From the material boundary thus defined, 3600 points evenly spaced around the circumferential line were extracted for each intrinsic characteristic, and the ideal feature of the type circle associated to the points using the least-squares fitting method.

Table 2. Control parameters and values used for studying CT dimensional measurement performance.

Part / Setup	V	I	S	t	G	A	B	P	Vx
POM40.0.01	110	450	50	1,0	16x	1	2x2	800	53
POM40.0.02	110	*900*	*99*	*0,5*	16x	1	2x2	800	53
POM40.0.03	110	*900*	*99*	*0,5*	16x	1	2x2	800	53
POM40.0.04	110	*225*	*25*	*2,0*	16x	1	2x2	800	53
POM40.0.05	110	450	50	*2,0*	*08x*	1	2x2	800	53
POM40.0.06	110	450	50	*0,5*	16x	*2*	2x2	800	53
POM40.0.07	110	450	50	1,0	*08x*	*2*	2x2	800	53
POM40.0.08	110	450	50	1,0	16x	1	2x2	*200*	53
POM40.0.09	110	450	50	1,0	16x	1	2x2	*400*	53
POM40.0.10	110	450	50	1,0	16x	1	2x2	*1200*	53
POM40.0.11	110	450	50	1,0	16x	1	*1x1*	*1600*	*27*
POM40.0.12	110	450	50	1,0	16x	1	2x2	800	*106*
POM40.0.13	110	450	50	1,0	16x	1	2x2	800	*213*
POM40.1.01	110	450	50	1,0	16x	1	2x2	800	53
POM40.1.02	110	450	50	*0,5*	16x	*2*	2x2	800	53
POM40.1.03	110	*900*	*99*	*0,5*	16x	1	2x2	800	53
POM60.0.01	120	450	54	1,0	16x	1	2x2	800	73
POM60.0.02	120	450	54	1,0	16x	1	2x2	800	*146*
POM60.0.03	120	450	54	1,0	16x	1	*1x1*	*1600*	*37*
POM60.1.01	130	450	58	1,0	16x	1	2x2	800	73
POM60.1.02	130	*900*	*117*	*0,5*	16x	1	2x2	800	73
POM60.2.01	130	350	46	1,0	16x	1	2x2	800	73
POM90.0.01	140	450	63	1,0	16x	1	2x2	800	106
POM90.0.02	140	450	63	1,0	16x	1	2x2	800	*213*
POM90.0.03	140	450	63	1,0	16x	1	*1x1*	*1600*	*53*
POM90.1.01	140	450	63	1,0	16x	1	2x2	800	106
POM90.1.02	140	*900*	*126*	*0,5*	16x	1	2x2	800	106
POM90.2.01	140	500	70	1,0	16x	1	2x2	800	106
POM90.3.01	140	500	70	1,0	16x	1	2x2	800	106
	Source voltage [kV]	Source current [µA]	Focal spot size [µm]	Sensor integration time [s]	Sensor sensitivity (gain)	Sensor image averaging	Sensor binning	Number of projections	Voxel size [µm]

2.4. Data analysis

In order to analyse the experimental data and comprehend how different volumetric matrices behave for each measured feature, *target average control chart* and *range control chart* were used. They allow verifying the statistical consistency of measured biases and variances for the different setups. The charts will evidence causal differences among the estimates, lowering the risk of wrong decisions about CT measurement data accuracy.

2.5. Good metrology practices

To allow the parts be easily and accurately positioned on the CT turntable, a stable mounting featuring a type II Kelvin

clamp [6] was designed and manufactured (shown in Fig. 2). The artefacts were orientated as illustrated in Fig. 2, with the revolution axis of the part parallel to the rotation axis of the turntable. During measurements, the part temperature inside the CT cabinet was monitored in order to properly correct its effect in the dimensional measurements.

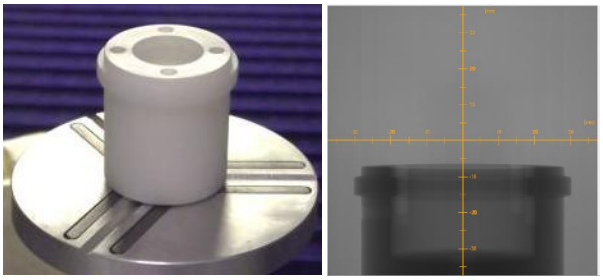

Fig. 2. Kinematic reference system with magnets, for easy, fast and repeatable mounting of the artefact (left) and projection (right).

In addition, manufacturer recommendations on qualifying various machine components were strictly followed or made more stringent: detector calibration (to homogenize the active detector field) on a weekly basis; geometric qualification (to soft-correct detector alignment errors) on a weekly basis; and turntable axis qualification (to soft-correct turntable axis drift and alignment errors).

3. EXPERIMENTAL FINDINGS

In this section, the most relevant findings for the intrinsic characteristics specified in 2.1 are graphically illustrated and analysed using target average control charts and range control charts.

3.1. Diameter of the external circumferential line, D_1

In Fig. 2, the range chart shows that no point is beyond the upper control limit, and thus a standard deviation on the order of 0.002 mm can be calculated. The estimated biases in the target average chart are clearly out of control, as the between-setup variation cannot be explained by the repeatability (i.e., within-setup variation). In fact, the highest points in the chart are related to those setups in which larger focal spot sizes and larger voxel sizes were applied.

However, those out-of-control setups do not regard some recommended practices in CT measurements, and thus they should be avoided in daily routine.

3.2. Diameter of the internal circumferential line, D_2

In Fig. 3, the range chart shows that no point is beyond the upper control limit, and thus a standard deviation on the order of 0.002 mm can be calculated. This value is similar to that calculated for D_1, since the least-squares association method was used for both diameters.

Here also the estimated biases in the target average chart are clearly beyond the limits, since the within-setup variation cannot explain the between-setup variation. In fact, the lowest points in the chart are related to those setups in which larger voxel sizes and larger focal spot sizes were applied. Comparing the bias charts relative to both diameters (upper chart in Fig. 2 and Fig. 3), it is apparent that the values are mirrored and slightly shifted.

However, those out-of-control setups do not regard some recommended practices in CT measurements, and thus they should be avoided in daily routine.

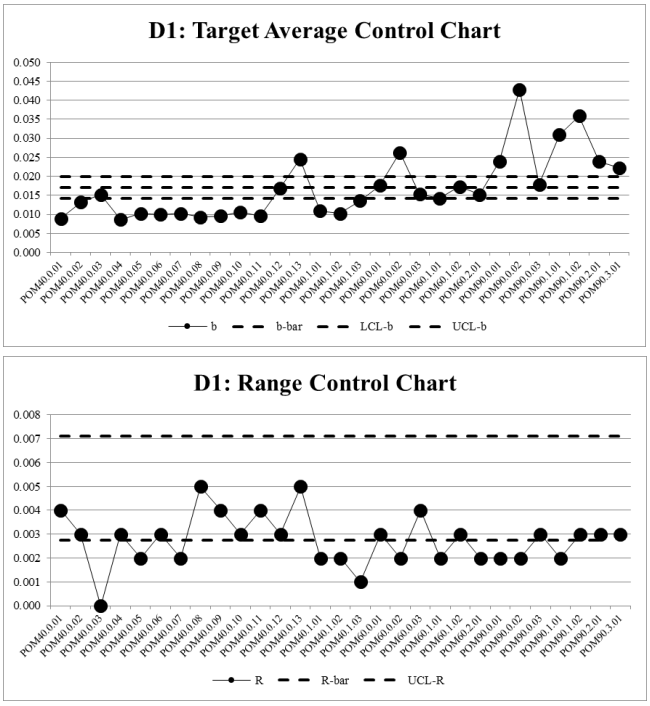

Fig. 2. Control chart for biases (upper) and control chart for ranges (lower) for the diameter of the external circumferential line.

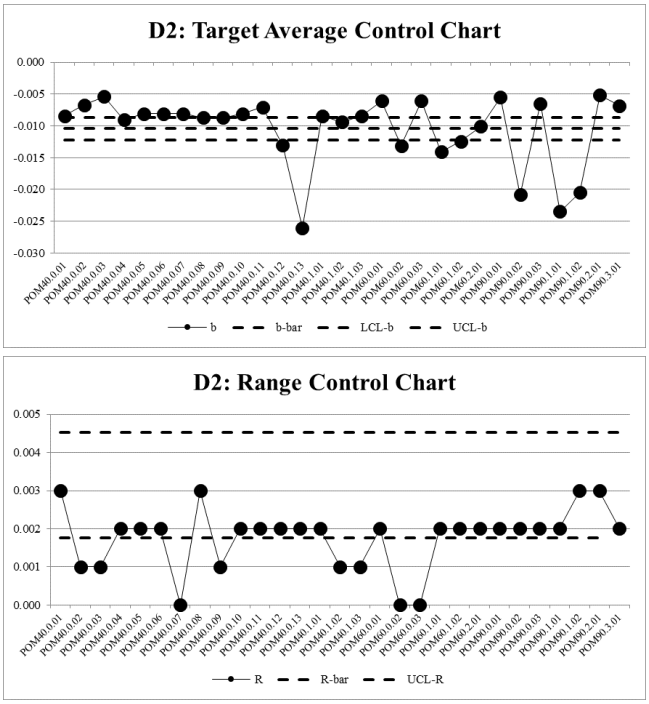

Fig. 3. Control chart for biases (upper) and control chart for ranges (lower) for the diameter of the internal circumferential line.

3.3. Diameter of the hole pattern, D_3

For the diameter of the circle associated to centres of the hole pattern, in principle, not influenced by edge offset errors, the range control chart displayed in Fig. 4 is under statistical control. The estimated bias in the target average chart is again

out of control, due to significant differences between results obtained with larger voxel sizes and larger focal spot sizes.

Removing the point related to part/setup POM90.0.02, in which a voxel size of 213 µm resulted (lower magnification), a smaller variation between setups could be verified than that observed in both D_1 and D_2. This is a consequence of nearly non-influence of edge detection effects.

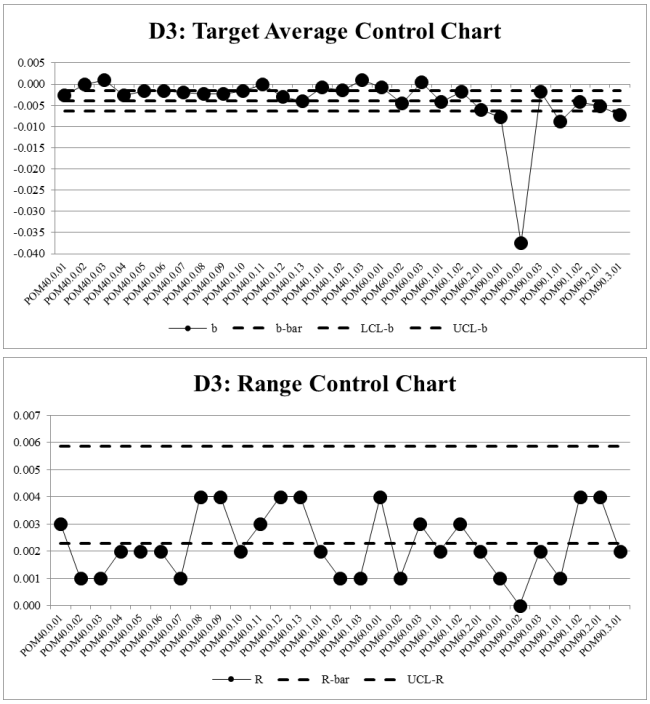

Fig. 4. Control chart for biases (upper) and control chart for ranges (lower) for the diameter of the circle associated to centres.

3.4. Roundness of the external circumferential line, R_1

In Fig. 5, the range chart displays three points beyond the upper limit, which are related to parts/setups POM40.0.13, POM60.0.03 and POM60.1.01. Despite the first outlier would be explained by the relative large voxel size, the other outliers would not be expected and would require more investigations to confirm that finding.

The estimated biases in the target average chart are clearly out of control, since the between-setup variation cannot be explained by the within-setup variation. In fact, the lowest values for each modular test artefact size are related to setups that used maximum detector resolution of 2048^2 pixels and a larger number or projections. On the other hand, the highest values are related to larger voxel sizes and angular steps.

The roundness value of the external circumferential line is dominated by the background noise presented in the CT data. When compared with the reference roundness value, a factor of ten could be evidenced, which might jeopardize profile and form evaluations, including CAD comparison, and any other analysis which relies on the extreme points.

3.5. Roundness of the internal circumferential line, R_2

The range chart shown in Fig. 6 displays an outlier related to part/setup POM40.0.13, expected due to the voxel size. The estimated biases in the target average chart are clearly out of control, as the between-setup variation cannot be explained by the within-setup variation. The other comments drawn to R_1 also apply to this intrinsic characteristic.

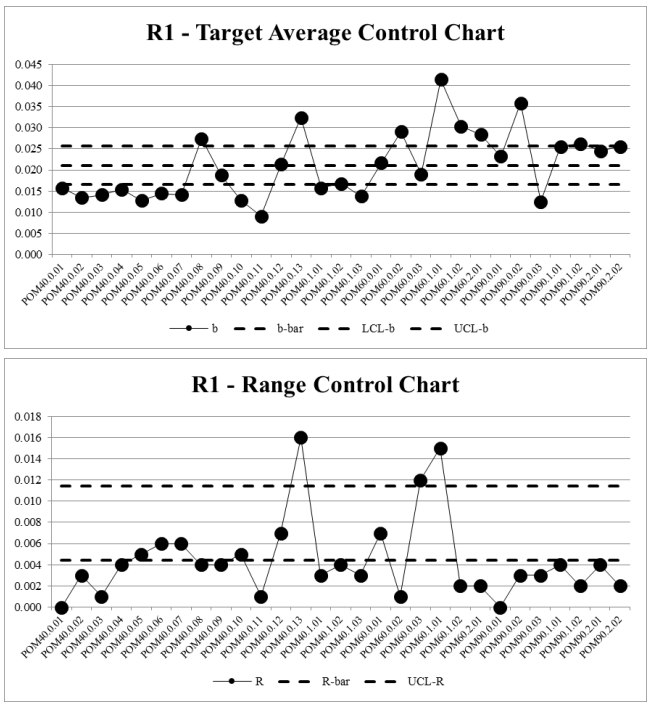

Fig. 5. Control chart for biases (upper) and control chart for ranges (lower) for the roundness of the external circumferential line.

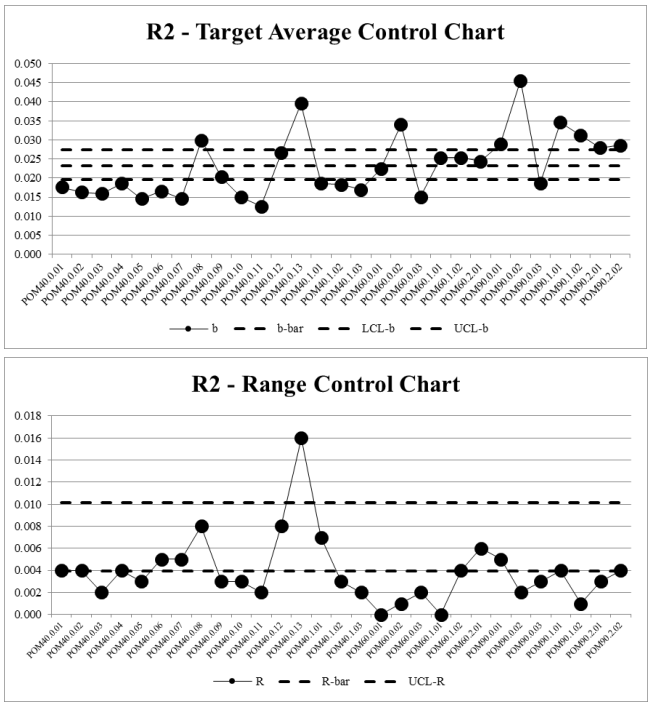

Fig. 6. Control chart for biases (upper) and control chart for ranges (lower) for the roundness of the internal circumferential line.

4. DISCUSSION AND FURTHER ANALYSES

The first inference that could be drawn from the study was the bias differences for external and internal features, which may be a direct consequence of edge detection errors. Being of systematic nature, they could be corrected using calibrated workpieces or accounted for in the measurement uncertainty. In the latter case, regarding the overall variation on the order of ± 0.03 mm, uncertainties in this range could be stated for measurements performed on parts with similar material and

shape. This becomes more evident by plotting all biases on a single chart, as shown in Fig. 7 and Fig. 8 (respectively, prior to and after removing biases related to unsuitable measuring practices, as discussed before). In Fig. 8, the highest point for D_1 (lowest for D_2) is associated with part/setup POM90.1.01, which featured the largest penetration length.

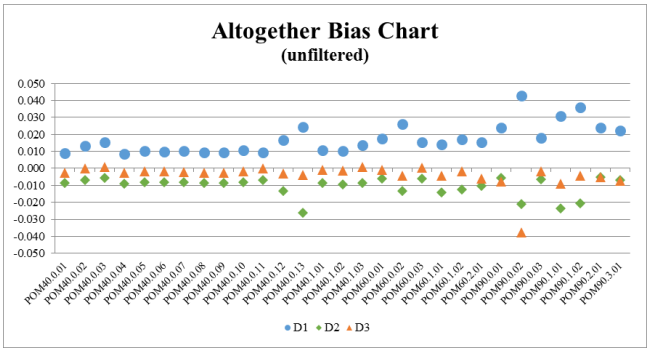

Fig. 7. Plotting of all biases before removal of outliers showing the measurement trend for distinct diameter characteristics.

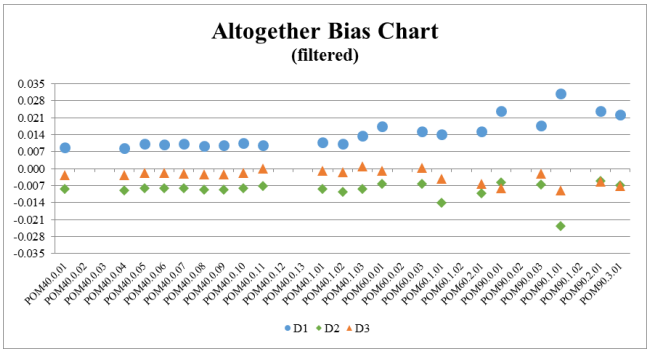

Fig. 8. Plotting of all biases after removal of outliers showing the measurement trend for distinct diameter characteristics.

In attention to the reference values for filter plate selection stated in the operating instructions of the metrological CT scanner, the base parametrization was repeated attaching filter plates at the outlet of the X-ray tube. For POM40 and POM60, a Cu-filter plate of 0.25 mm was used; for POM90, a Cu-filter plate of 0.5 mm was selected. Fig. 9 illustrates the estimated biases for D_1 and D_2. In general, the use of a pre-filter slightly minimizes the bias for POM40 and POM60. For part/setup POM90.1.01, substantial offset reduction could be evidenced when using a Cu-filter plate, which demonstrates the critical role of placing pre-filters when inspecting larger parts.

From the experimental investigation, other lessons could be learnt for more reliable dimensional evaluation of features of size: (a) the focal spot size should be closer or smaller than the voxel size; (b) the detector gain setting would not affect average size, albeit increasing the gain would result in noisier images; (c) the smaller the angular increment, the lesser the image background noise; (d) the higher the image resolution, the lesser the image background noise; and (e) the higher the magnification factor, the lower the measured biases.

5. CONCLUDING REMARKS AND OUTLOOK

In principle, the error limit determined would be valid for the metrological CT system under test. That is a value beyond the maximum permissible error stated by the manufacturer, as it is nearly insensitive to edge detection errors and material influence. From the measurement application point of view, that error limit would be more representative and reasonable for most dimensioning tasks performed on plastic parts.

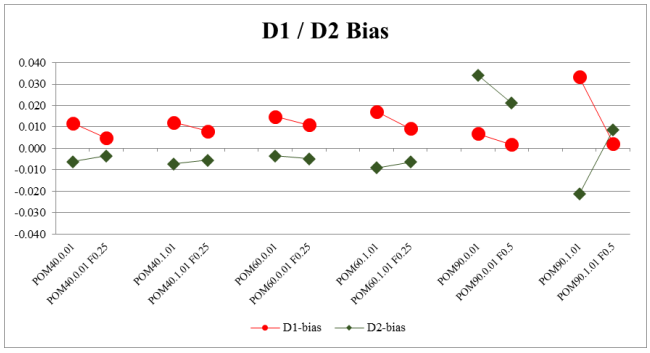

Fig. 9. Plotting of the estimated biases for diameters D_1 and D_2 when using a filter plate attached at the outlet of the X-ray tube.

Though more tests may be needed to refine the error limit range, it is very important to mention that generic uncertainty statements are in accordance with technical standards such as ISO 10012 and ISO 14253-2. Those tests could be carried out on calibrated production plastic parts, and CT measurements compared with reference values. The resulting biases would strengthen the generic uncertainty statement. In any case, it should be borne in mind that the lesson learning process is also part of the uncertainty estimation task.

Future works will also involve estimating uncertainties for dimensioning parts made of light metals such as aluminium. In principle, a similar experimental design could be applied. However, due to higher energy requirements for penetrating light metals, the use of filter plates will be even more critical, from a certain part size, to improve the radiation spectrum and reduce beam-hardening effects. That would contribute to the measurement uncertainty, as the selection of filter plates and later parametrization is operator-dependent.

REFERENCES

[1] J. P. Kruth, et al., “Computed tomography for dimensional metrology”, *CIRP Annals*, vol. 60, no. 2, pp. 821-842, 2011.

[2] F. A. Arenhart, et al., “Investigation of CT-induced random surface deviations using a multi-wave standard”, *Conference on Industrial Computed Tomography (ICT)*, Wels, Austria, September 19-21, 2012.

[3] V. C. Nardelli, et al., “Modular test parts to assess the quality of CT dimensional measurements”, *Conference on Industrial Computed Tomography (ICT)*, Wels, Austria, September 19-21, 2012.

[4] H. Lettenbauer, et al., “Means to verify the accuracy of CT systems for metrology applications (in the absence of established international standards)”, *International Symposium on Digital Industrial Radiology and Computed Tomography (DIR)*, Lyon, France, June 25-27, 2007.

[5] M. Bartscher, et al., “Coordinate metrology using computed tomography systems - an overview of PTB's activities with a focus to standardization”, *Industrial CT Scanning German-Austrian-Danish Workshop*, Munich, Germany, October 23-25, 2013.

[6] R. K. Leach, *Fundamental principles of engineering nanometrology*, Elsevier, Oxford, 2010.